Politecnico
di Torino

Politecnico di Torino

Master of Science in Energy and Nuclear Engineering
01FJIXY - Computational Thermomechanics
A.Y. 2025/2026

Homework 04 - Pressure Vessel

Tommaso COGOZZO

1 Problem statement and given data

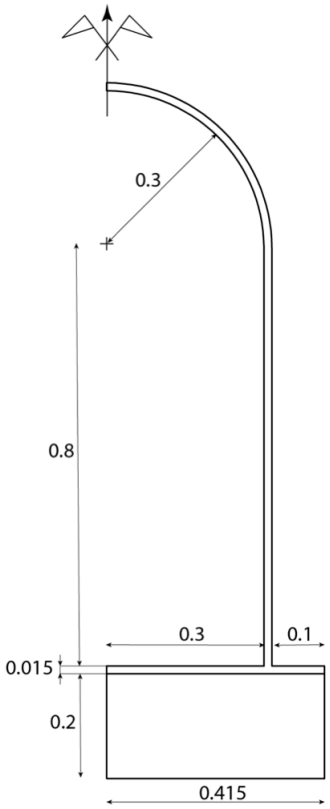

Figure 1: Pressure vessel with uniform pressure inside

Data:

- Vessel thickness: $t = 0.015\,m$
- Poisson's ratio: $\nu = 0.3$
- Elasticity modulus: $E = 2.1e11\,N/m^2$
- Applied internal pressure: $p = 7.0e6\,Pa$

2 Objective

The proposed problem involves the finite element (FEM) analysis of a cylindrical pressure vessel mounted on a parallelepiped base and closed at the upper end by a hemispherical cap. Owing to the axial symmetry of the vessel and its uniform wall thickness, only one quarter of the entire domain can be considered, provided that appropriate symmetry boundary conditions are applied.

By further exploiting the geometric characteristics of the system to simplify the analysis, the computational domain can be subdivided into three main subdomains: the base support, the cylindrical shell, and the hemispherical cap. This subdivision facilitates the finite element discretization process and allows for the correct application of boundary conditions and mechanical constraints on each individual region.

From classical pressure vessel theory, it is known that for the cylindrical section of pressure vessels, the circumferential stress σ_c, the axial stress σ_a, and the radial stress σ_r can be readily evaluated using the following relationships[1]:

$$\sigma_c = \frac{pr}{t}$$
$$\sigma_a = \frac{pr}{2t}$$
$$\sigma_r = 0$$

For the hemispherical end of the pressure vessel, the corresponding stress components can be determined using the following relationships:

$$\sigma_c = \frac{pr}{2t}$$
$$\sigma_a = \frac{pr}{2t}$$
$$\sigma_r = 0$$

The purpose of this study is to investigate the numerical solution of the pressure vessel problem described above by means of the Finite Element Analysis Program (FEAP). The analysis aims to evaluate the stress distribution within the structure and to assess the capability of the numerical model to reproduce the theoretical predictions derived from classical pressure vessel theory.

To this end, the problem is solved using two different discretization strategies in order to compare their numerical performance and accuracy. In particular, linear triangular elements (three nodes elements) and linear quadrilateral elements (four nodes elements) are employed. The comparison between these two element types allows for an evaluation of the influence of mesh topology on the quality of the numerical results, as well as on the convergence behavior of the finite element solution.

[1]The above relationships are valid under the thin-walled cylinder assumption, that is, for cylinders in which the wall thickness is small compared to the internal diameter. According to the most commonly adopted international convention, circular cylinders are classified as thin-walled when the ratio between the wall thickness s and the internal diameter d_i is less than or equal to $1/20$. In the present case, the ratio satisfies this condition, with $s/d_i = 1/20$.

3 Finite Element Analysis with Triangular Plane Stress Elements

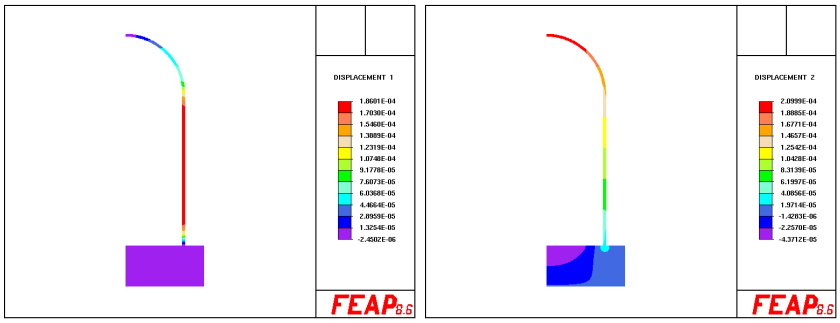

(a) Radial displacement (b) Axial displacement

Figure 2: Computed radial and axial displacement color map with mr = 10

The contour plots of the radial and axial displacements allow for the verification of the correct implementation of the axisymmetric symmetry boundary conditions. The adoption of a reduced computational domain implies that the corresponding boundary surfaces must be constrained by means of sliding roller boundary conditions.

This requirement is satisfied, as shown in Fig.2a, where the radial displacement is observed to be zero both at the base of the pressure vessel and at the apex of the hemispherical cap. Furthermore, the axial displacement field reported in Fig.2b appears smooth, continuous, and symmetric along the planes of symmetry, with no spurious discontinuities or localized perturbations.

Taken together, these observations confirm that the reduced axisymmetric model adequately represents the full pressure vessel geometry.

The figures below present the contour plots of the radial, axial, and circumferential stress components for the cylindrical portion of the pressure vessel, obtained using a mesh refinement level equal to 2. In agreement with the theoretical prediction, which yields a zero value, the radial stress along the cylindrical surface is also found to be $\sigma_r = 0$ in the numerical solution, as shown in the corresponding contour plot.

For the same discretization level, the numerical results provide values of $\sigma_a = 7.48 \times 10^7\,\mathrm{N/m^2}$ and $\sigma_c = 1.46 \times 10^8\,\mathrm{N/m^2}$. These values are in good agreement with the corresponding theoretical stresses, which are $\sigma_a = 7.00 \times 10^7\,\mathrm{N/m^2}$ and $\sigma_c = 1.40 \times 10^8\,\mathrm{N/m^2}$, respectively. The relative error with respect to the analytical solution is approximately 6.9% for the axial stress and 4.3% for the circumferential stress.

An additional relevant observation concerns the uniformity of all three stress components throughout the cylindrical domain under consideration, which is consistent with the assumptions of thin-walled pressure vessel theory.

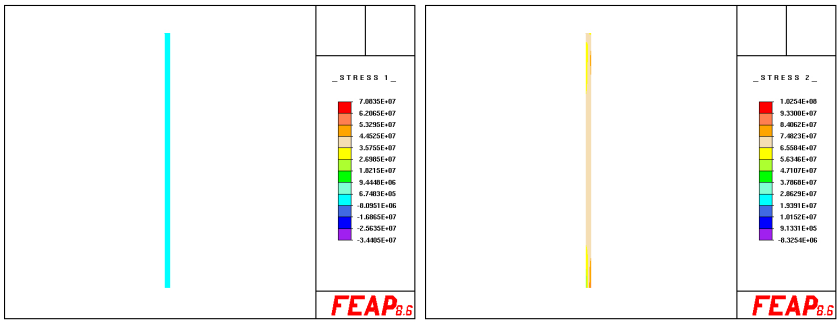

(a) Radial stress σ_r (b) Axial stress σ_a

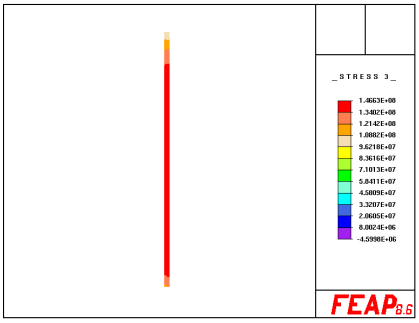

(c) Circumferential stress σ_c

Figure 3: Computed stresses color map with mr = 2 for cylindrical domain

For the hemispherical end of the pressure vessel, the theoretical value of the circumferential stress is evaluated as $\sigma_c = \dfrac{pr}{2t} = 7.00 \times 10^7 N/m^2$. Figure 4 shows the contour plot of the circumferential stress σ_c for the hemispherical portion of the pressure vessel. In this case, the numerical solution yields a value of $\sigma_c = 7.10 \times 10^7\,\mathrm{N/m^2}$, which appears to be nearly uniform over the entire hemispherical domain.

The corresponding relative error with respect to the theoretical value is approximately 1.4%, indicating that the obtained result can already be considered accurate, despite the relatively low level of mesh refinement employed in the analysis.

Before concluding the FEM analysis using linear triangular elements, the same computational procedure was repeated by adopting a mesh refinement level equal to 10. As shown in Fig. 5, the following numerical values were obtained:

- $\sigma_r = 0\,\mathrm{N/m^2}$,
- $\sigma_a = 8.45 \times 10^7\,\mathrm{N/m^2}$,
- $\sigma_c = 1.47 \times 10^8\,\mathrm{N/m^2}$ for the cylindrical section,

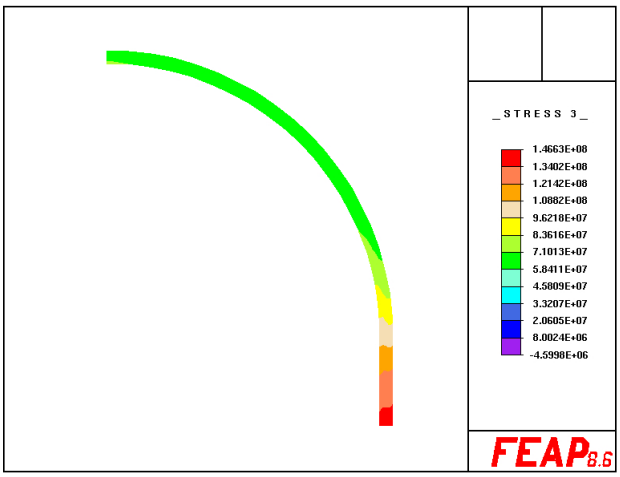

Figure 4: Circumferential stress on the hemispherical end of pressure vessel (mr = 2)

- $\sigma_c = 6.80 \times 10^7\,\mathrm{N/m^2}$ for the hemispherical end.

Although an improvement in accuracy was expected with the increased mesh refinement, given that the results obtained with a refinement level of 2 were already acceptable, the numerical solution does not exhibit a closer agreement with the theoretical values. On the contrary, the computed stresses appear to deviate further from the analytical predictions.

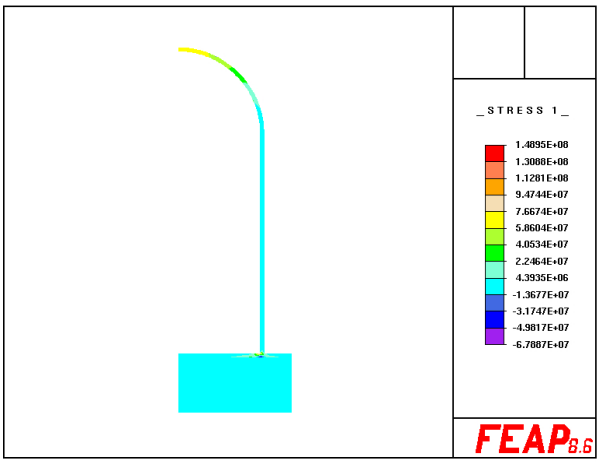

(a) Radial stress σ_r

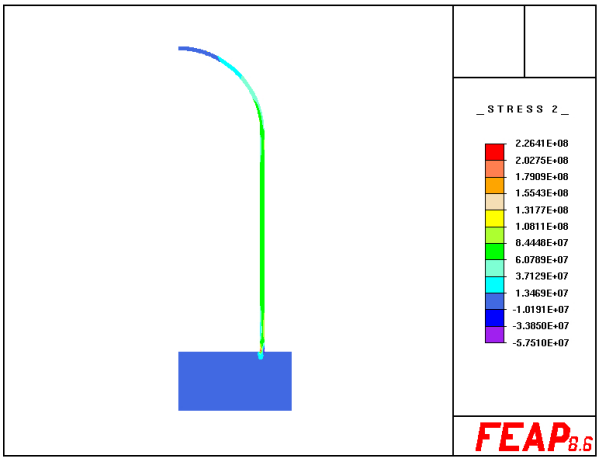

(b) Axial stress σ_a

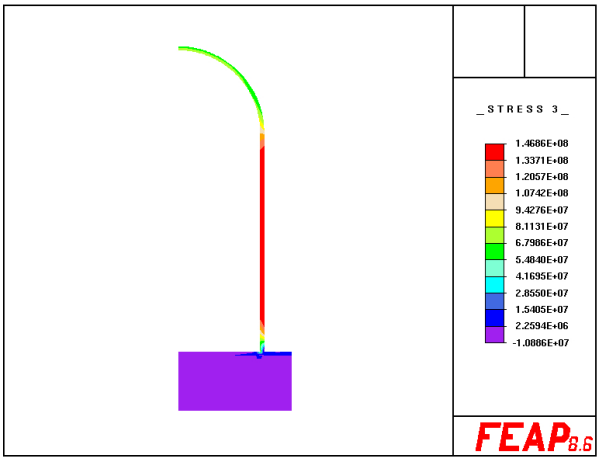

(c) Circumferential stress σ_c

Figure 5: Computed stresses color map with mr = 10

4 Finite Element Analysis with Rectangular Plane Stress Elements

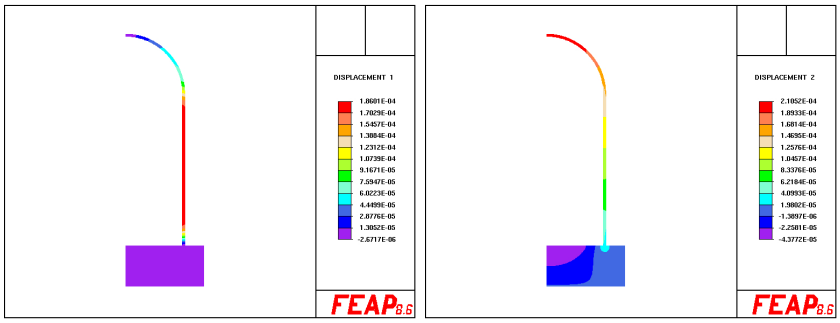

(a) Radial displacement (b) Axial displacement

Figure 6: Computed radial and axial displacement color map with mr = 10

Before proceeding with the FEM analysis of the stresses acting on the pressure vessel using linear quadrilateral elements, it is necessary to repeat the verification of the radial and axial displacement fields associated with the implementation of the symmetry boundary conditions.

As shown in Fig.6, the radial displacement is observed to be zero in the vicinity of both the base of the pressure vessel and the apex of the hemispherical closure, while the axial displacement exhibits a smooth and uniform distribution throughout the domain. These observations confirm that the symmetry boundary conditions are correctly enforced also in the case of linear quadrilateral elements. Consequently, the outcome of the displacement verification can be considered satisfactory.

By discretizing the computational domain using linear quadrilateral elements, the numerical values of the stress components acting on the pressure vessel under investigation were evaluated. The results reported below represent the stress distribution obtained from the finite element analysis and allow for a direct comparison with both the analytical solution derived from classical pressure vessel theory and the results previously obtained using linear triangular elements.

- $\sigma_r = 0\,\mathrm{N/m^2}$,
- $\sigma_a = 7.26 \times 10^7\,\mathrm{N/m^2}$,
- $\sigma_c = 1.47 \times 10^8\,\mathrm{N/m^2}$ for the cylindrical section,
- $\sigma_c = 7.05 \times 10^7\,\mathrm{N/m^2}$ for the hemispherical end.

It is evident that the numerical values obtained using linear quadrilateral elements exhibit an excellent agreement with the corresponding analytical solutions. For an equivalent level of mesh refinement, the discretization based on

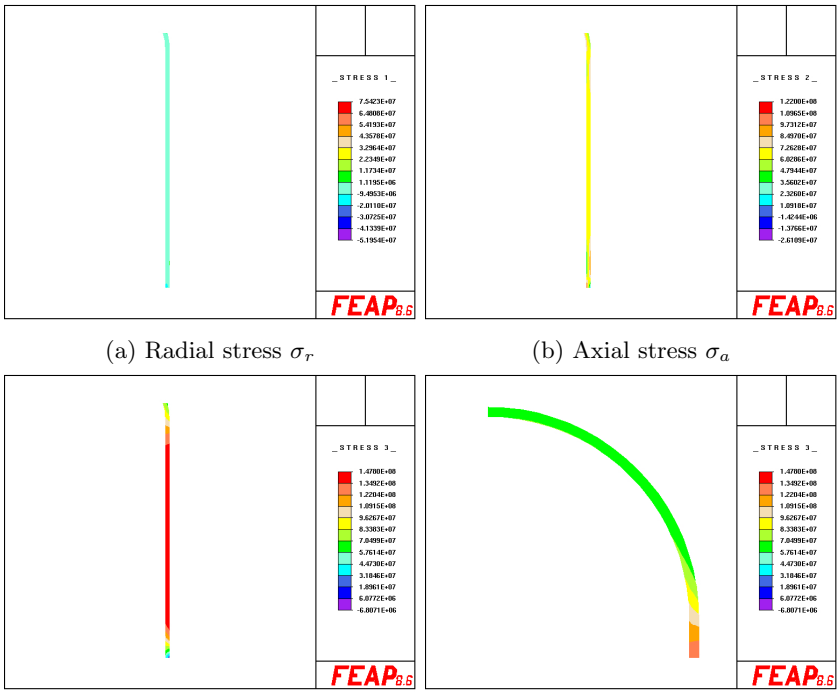

(a) Radial stress σ_r (b) Axial stress σ_a

(c) Circumferential stress σ_c (d) Circumferential stress σ_c

Figure 7: Computed stresses color map with mr = 2 for cylindrical body

linear quadrilateral elements proves to be more accurate than the one employing linear triangular elements, highlighting the superior performance of this element type for the problem under consideration.

An additional important outcome of the analysis is the uniformity of the computed stress components over the examined surfaces, as clearly shown by the contour plots reported in Fig.7. This behavior is fully consistent with the assumptions of classical pressure vessel theory, which predict constant stress distributions in thin-walled cylindrical and hemispherical structures subjected to internal pressure. These results further confirm the reliability and adequacy of the adopted finite element model.

In order to reproduce the same analysis presented in the previous section, the mesh refinement level was increased to 10. The resulting numerical values obtained from the finite element analysis are therefore reported below:

- $\sigma_r = 0\,\mathrm{N/m^2}$,
- $\sigma_a = 8.30 \times 10^7\,\mathrm{N/m^2}$,
- $\sigma_c = 1.46 \times 10^8\,\mathrm{N/m^2}$ for the cylindrical section,
- $\sigma_c = 7.96 \times 10^7\,\mathrm{N/m^2}$ for the hemispherical end.

Also in this case, it must be concluded that the adoption of a more refined discretization does not lead to an improvement in the accuracy of the numerical results. On the contrary, the use of a finer mesh produces stress values that deviate further from the corresponding analytical solutions. This outcome suggests that, beyond a certain level of refinement, the accuracy of the solution is no longer governed by the mesh density alone, but is instead influenced by other factors such as the element formulation and the numerical characteristics of the finite element approximation.

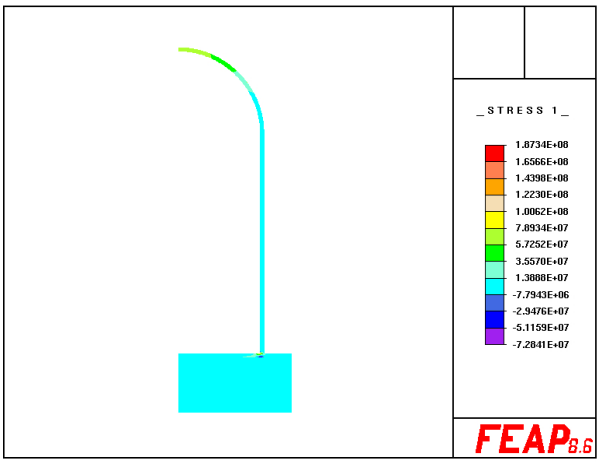

(a) Radial stress σ_r

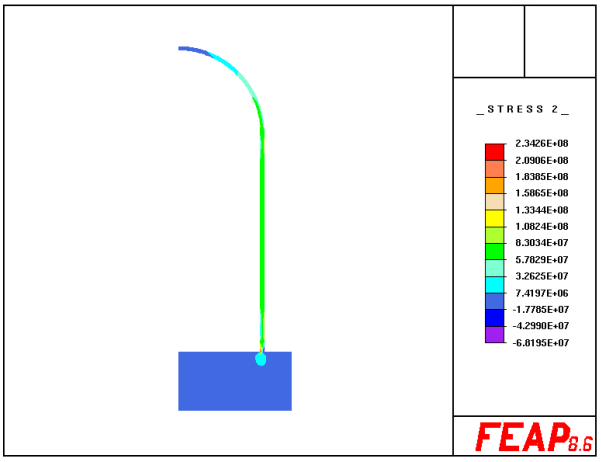

(b) Axial stress σ_a

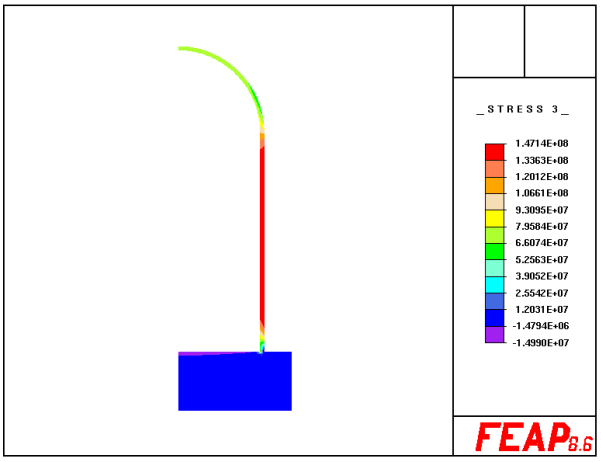

(c) Circumferential stress σ_c

Figure 8: Computed stresses color map with mr = 10

5 Conclusion

The finite element analysis carried out in this study allowed for a comprehensive evaluation of the stress state in a thin-walled pressure vessel by comparing different discretization strategies and mesh refinement levels. The numerical results were systematically assessed against the analytical solutions provided by classical pressure vessel theory, enabling a clear validation of the adopted modeling approach.

Among the discretization techniques considered, the use of linear quadrilateral elements proved to be the most effective. For an equivalent mesh refinement level, this element formulation consistently yielded numerical stress values that were in closer agreement with the analytical predictions compared to those obtained using linear triangular elements. Furthermore, the stress fields computed with linear quadrilateral elements exhibited a high degree of uniformity over both the cylindrical and hemispherical regions of the pressure vessel, in full accordance with the assumptions underlying thin-walled pressure vessel theory. These observations confirm the superior accuracy and reliability of linear quadrilateral elements for the present class of problems.

An additional and noteworthy outcome of the analysis concerns the influence of mesh refinement on the accuracy of the numerical solution. Contrary to the intuitive expectation that a finer mesh would necessarily improve the results, it was observed that a relatively low mesh refinement level ($\mathrm{mr} = 2$) provided numerical solutions that were already remarkably accurate and, in several cases, closer to the analytical values than those obtained with a significantly finer discretization ($\mathrm{mr} = 10$). This behavior suggests that, beyond a certain refinement threshold, the accuracy of the solution is no longer governed solely by mesh density, but is instead affected by factors such as element formulation, numerical integration, and stress recovery procedures.

In conclusion, the present study demonstrates that an appropriate choice of element type plays a more critical role than excessive mesh refinement in achieving accurate and physically consistent results. In particular, linear quadrilateral elements combined with a moderate mesh refinement level represent an optimal and computationally efficient solution for the finite element analysis of thin-walled pressure vessels.